Design and Operation of MW-Class MPD Thrusters Part I: Numerical Modeling[1]

Pavlos G. Mikellides
Ohio Aerospace Institute
22800 Cedar Point Dr.
Cleveland, OH 44142
(440) 962-3164
PavlosMikellides@oai.org

IEPC-01-124

The magnetohydrodynamic code, MACH2 is utilized to investigate MW-class, self-field magnetoplasmadynamic thrusters. The numerical results are validated by comparisons to experimental data and offer significant insights at this regime of operation. Specifically, operation at 0.5-6MW and 1.37 g/s shows incomplete hydrogen-propellant ionization that is dominated by electron-neutral collisions which in turn increase the plasma voltage, but do not substantially increase thrust. Detailed interrogation of energy deposition shows significant deposition to internal modes - as opposed to electrode losses via fall voltage and thermal conduction - even at the higher power levels. These frozen-flow losses can be converted to axial thrust by proper expansion of the flow.

Introduction

Electromagnetic acceleration with and without externally applied magnetic fields has traditionally been a very attractive concept for a variety of space missions ranging from orbital maneuvering to interplanetary travel. The basic acceleration mechanisms are two-fold; the relative significance of each force component depends on the power-level and mass-flow-rate operation. The current generated by the applied voltage differential between the electrodes induces an azimuthal magnetic field which in turn interacts with the current to produce an axially-directed electromagnetic force, known as the Lorentz force. (See Fig. 1) In addition, the applied current heats the plasma via Ohmic heating which generates an electrothermal-force component as the gas expands to vacuum conditions. The thruster is relatively simple to operate within a robust configuration that diminishes component failure and maintenance issues. It can provide intermediate values for specific impulse (2000-7000 sec) and thrust that compete with both chemical-aerobraked and electrothermally-dominated systems as well as ion and hall thrusters.

The self-field magneto-plasmadynamic (MPD)

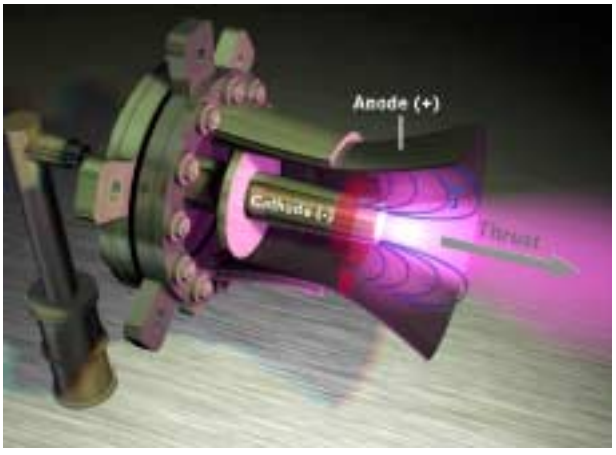

Figure 1. Representative schematic of the self-field magnetoplasmadynamic thruster with basic acceleration mechanism.

[1] Presented as Paper IEPC-01-000 at the 27th International Electric Propulsion Conference, Pasadena, CA, 15-19 October, 2001.

thruster however, has to consistently operate at efficiencies exceeding 50% and demonstrate the necessary lifetimes to provide the payload and trip-time advantages associated with the aforementioned performance capabilities.[1, 2] Even though it has been rigorously researched for the last forty years, such efficient implementation still eludes us. To date, our accomplishments and understanding of self-field MPD operation are limited to the following, largely empirical findings:

Performance improves with increasing power levels; the highest reported cases demonstrated 40% efficiency at 1.5 MW[3] and 55% at 15 MW.[4] The inefficiencies have been attributed to frozen-flow and electrode losses through fall voltage and thermal conduction. Furthermore, the self-field MPD thruster demonstrates a limitation as power is increased, the so-called "onset", that is accompanied by voltage fluctuations and elevated electrode erosion.[4] This phenomenon, which scales with the current squared over the mass-flow rate among other parameters, degrades performance at higher power levels and substantially limits the thruster's lifetime. The latter is indeed the ultimate performance ceiling. Missions of interest require operation in the thousands of hours while the longest demonstrated test did not exceed 500 hrs.

Rigorous theory is necessary to provide the insights that may lead to overcoming onset limitations and properly develop magnetic nozzles, thus providing optimized configurations. The magneto-hydrodynamic code, MACH2 has been previously utilized to examine applied-field MPD acceleration with great success. Besides being a full 2-D, axisymmetric code that can simulate real thruster geometries and real plasmas, it includes unique transport models that have been essential in deciphering operation at the 100 kW level. Specifically, this previous research has completely altered the traditional perception of magnetic nozzle operation, but most importantly suggested that future work should concentrate in identifying regimes that are not dominated by anomalous transport. Preliminary analysis suggests that applied-field operation at higher power levels may offer such environment due to the necessary higher mass-flow operation.

This paper concentrates in modeling self-field operation in the MW-power levels using the MACH2 code. The main objective is to validate the model by comparing to experimental data and attempt to provide useful insights by accounting the power deposition into the possible energy sinks.

Numerical Model

In the mid-1980s the Mission Research Corporation developed a magnetohydrodynamics (MHD) code under Air Force contract to study collisional plasmas for problems of complex geometries.[5] Over the years, this Multi-block Arbitrary Coordinate Hydromagnetic (MACH) simulation tool has been utilized to model a diverse range of plasma problems and has been substantially upgraded through contributions from a variety of scientists. It is currently being maintained and upgraded to a three-dimensional solver (MACH3) by The Center for Plasma Theory and Computation at the Air Force Research Laboratory.

MACH2 is a time-dependent, two-dimensional, axisymmetric, multi-material code that can be applied to problems of complex geometries due to its multi-block structure.[6] The computational mesh can move in an Arbitrary-Lagrangian-Eulerian (ALE) fashion allowing applicability to both diffusive- and dispersive-dominated problems as well as code validation. The mesh can be refined via a variety of adaptive schemes to capture regions of varying characteristic scale. The set of the single-fluid, MHD equations is time-advanced with finite-volume spacial differencing, and the boundary conditions are applied via the ghost-cell technique so that no special conditional statement is necessary at the boundaries.

The mass continuity and momentum equations assume a compressible, viscous fluid with the latter including both real and artificial viscosity effects. The stress-deviator can be chosen to evolve under elastic stress for strength of material calculations[7] or modeled as a Newtonian fluid to upgrade the code to a Navier-Stokes solver.[8] The code includes two ablation models that allow mass addition due to solid evaporation and have been successfully employed to model ablation-fed pulsed plasma

thrusters.[9] The electrons, ions and radiation field are in thermal non-equilibrium, so MACH2 solves three energy equations. These include thermal conduction with anisotropic transport[10] and three different models for radiation cooling.[21,11] Evolution of the magnetic field is prescribed by the induction equation that includes resistive diffusion, the Hall effect and the thermal source for magnetic fields. Various models for the plasma resistivity are available. They comprise classical anisotropic resistivity,[26] several anomalous resistivity models and contributions from electron-neutral collisions applicable to weakly ionized gases.[21] In many engineering applications the source of magnetic flux is applied currents produced from externally-applied voltage differentials. For this, the code includes a variety of circuit models such as LRC, Pulse-Forming-Networks, sine-waveforms and several others. Other additional physical models include laser-pulse energy deposition and a detonation package.

The set of the MHD equations is completed by an equation of state that can be either analytic or tabular. The latter is provided by the SESAME library that includes semi-empirical models for the thermodynamic properties, transport coefficients, (including opacities) and average ionization state under local thermodynamic equilibrium. These models have been constructed and are being maintained by the T-1 and T-4 groups at Los Alamos National Laboratory.[12]

The level of sophistication and capability of the MACH2 code has been instrumental in providing invaluable insights to a variety of plasma problems. Some of these include plasma opening switches,[13] inertial-confinement fusion and alternative concepts,[14] compact toroid formation and acceleration schemes,[15] gas and solid density z-pinch implosion physics,[16] laser-target interactions,[17] high-power plasma source design,[18] magnetic nozzles[19] and a variety of plasma thrusters.[12,18] Its diverse success establishes the code as a primary numerical tool toward the understanding and development of efficient, MW-class MPD thruster designs.

MW-Class, Self-field MPD Simulations

In an effort to provide code validation and useful insights, MACH2 was employed to model real MW-class thrusters in order to compare to experimental data. The particular thruster selected for the simulations was one of the Japanese MY[20,21] family of MPD configurations that was operated with and without external magnetic fields. In this manner, MACH2 could be compared to both self-field and eventually applied-field operation within the power levels of interest.

Experimental Overview

The simulations examined the MY-II version[21] of the thruster a schematic of which is shown in Fig. 2-top along with the relative dimensions. The cathode was constructed of thoriated tungsten, ($2.8V<\Phi_{Th-W}<3V$) and the anode was mostly copper ($\Phi\sim4.7V$) interjected by 1-mm slits filled with ceramic material. It was operated with Hydrogen propellant injected at a 50:50 ratio through two gas-feed ports adjacent to the electrodes, (See Fig.1) at a mass-flow rate of 1.37 g/s. The power supply provided a 0.6 msec pulse at a maximum of 62kJ which allowed thruster operation at quasi-steady current levels of 4kA-20kA corresponding to power levels of 0.5MW-6MW. The experimental data for self-field operation included thrust and discharge voltage along with B-probe measurements that allowed mapping of the current distribution for the 10kA case. In addition, erosion tests were performed that showed insignificant anode-material loss and Th-W cathode losses of the order of 230μg/shot (39.5μg/C). Even though these values are still significant relative to mission-of-interest durations, other cathode materials[22] were tested to show reduced erosion rates without affecting performance. Thermal characterization based on experimental measurements was also carried out mapping electrode surface temperature. The 10-kA analysis computed cathode surface temperatures in the range of 1600K-2600K and anode temperatures of 600K-1500K. No evidence of onset was observed in the regime of operation.

A preliminary analysis based on the behavior of the thruster implies operation at currents below nominal even at the maximum current level of 20kA. A

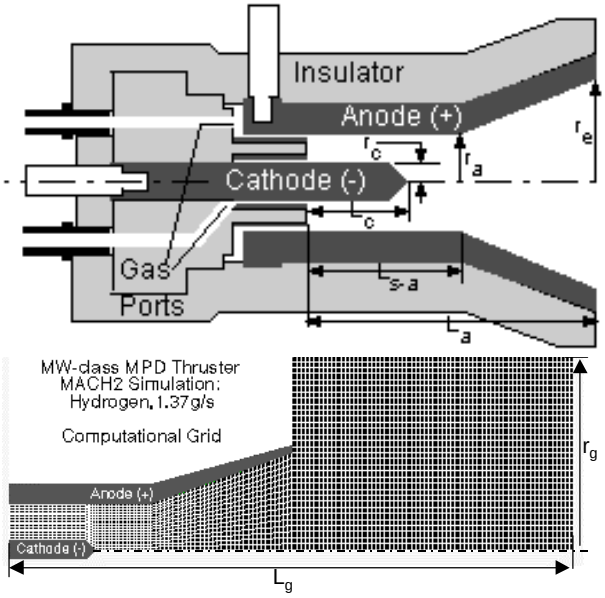

Figure 2. Top: Schematic of the multi-megawatt, MY-II MPD thruster used for the MACH2 simulations. Bottom: MACH2 computational region and grid. Dimensions in mm: r_c=4.75, r_a=25, r_e=52, L_c=45, L_{s-a}=75, L_a=104, L_g=300, r_g=104.

simple calculation of the power required to dissociate and fully ionize the hydrogen propellant (E_i = 15.4eV for H_2) at 1.37 g/s exceeds 2 MW which suggests that incomplete ionization should be expected.

Physical Modeling

The physics included in the MACH2 simulations modeled a viscous fluid with thermal non-equilibrium and real equation-of-state for monatomic hydrogen supplied by the SESAME tables. The latter includes the energy to dissociate, however it can't address possible regimes within which incomplete dissociation may be present. The thermodynamic properties include the average degree of ionization, ζ. The no-slip boundary condition was employed at the electrode surfaces while thermal conduction was assumed at a constant temperature of 2000K for the cathode and 1000K for the anode, consistent with the aforementioned experimentally-deduced data. Backplate mass injection employed a new parabolic-density scheme to approximate experimental mass feed in the vicinity of the electrodes. Mass was injected at sonic speeds for monatomic hydrogen at 300K. The computational region was extended well downstream of the thruster's exit, see Fig.1-bottom, in order to capture plume processes and impose uniform outlet boundary conditions, (i.e. zero-gradient boundary condition). Deposition of energy into different modes was calculated at the outlet boundaries in the following manner:

$$\text{Axial Thrust: } T_z = \int\left[p + \frac{B^2}{2\mu_o} + \rho u_z^2\right] dA_z \quad (1)$$

$$\text{Radial Thrust: } T_r = \int\left[p + \frac{B^2}{2\mu_o} + \rho u_r^2\right] dA_r \quad (2)$$

$$\text{Ionization Power: } P_{INZ} = \frac{E_i}{m_i}\int \rho\zeta\bar{u}\cdot d\bar{A} \quad (3)$$

$$\text{Thermal Power: } P_{THE} = \int \rho(e_H + e_e)\bar{u}\cdot d\bar{A} \quad (4)$$

$$\text{Thermal Conduction Power: } P_{TBC} = \int(\kappa_H \bar{\nabla}T_H + \kappa_e \bar{\nabla}T_e)\cdot d\bar{A}_{elctrds} \quad (5)$$

Axial, P_z and radial, P_r thrust power was deduced from eq.1 and 2, respectively by utilizing $P=T^2/2m$. The ionization energy per particle, E_i includes the energy to dissociate, i.e. E_i=15.4 eV, and thermal conduction power represents the losses to the electrodes modeled to conduct heat at constant temperature.

Current was assumed constant as the modeling focuses on steady-state operation which was computationally reached within 0.5-1 msec. This was confirmed by both the evolution of integrated variables and evolution of two-dimensional distributions to a constant value.

Flow Characterization

Comparisons of the steady state simulations to the experimental data for a discharge current of 10 kA (Fig. 3) were quite favorable and provided new insights that demanded further interrogation. Principally, they have identified the importance of electron-neutral collisions in this regime of operation, especially with respect to energy deposition. In particular, the plasma electrical diffusivity in MACH2 can be modeled to include contributions from such collisions as follows (shown in scalar form):

$$\hat{\eta} = 1.0328 \times 10^{-4} \frac{\zeta \ln \Lambda}{\mu_o T_e^{3/2}} + \frac{Q_{eA}(1-\zeta)}{\mu_o e \zeta} \sqrt{\frac{m_e T_e}{e}} \quad (m^2/s) \tag{6}$$

For Hydrogen the electron-neutral collision cross section, Q_{eA} was taken at 5×10^{-19} m^2 as a reasonable average over a range of electron energies.[22] The first term represents the classical Spitzer-Härm formulation while the second is additive and accounts for electron-atom collisions.

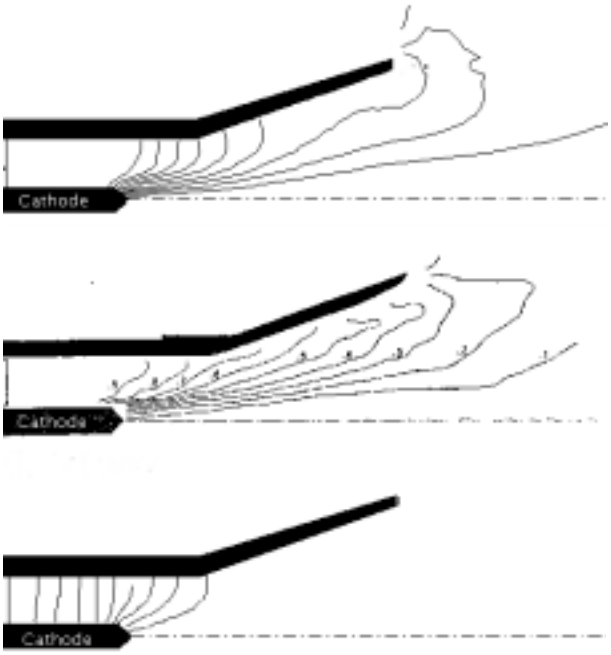

Figure 3. Current Distribution at 10kA. Each contour represents a 10% increment.
Top: MACH2 simulation with electron-neutral collisions included in the resistivity model. Thrust=36.9N, Voltage=183V.
Middle: Experiment, Thrust=34N, Voltage=200V, efficiency=21%.
Bottom: MACH2 simulation with classical resistivity, Thrust=32.4N, Voltage=108V.

Exclusion of such a contribution implied that the major energy losses are due to fall voltages and other external circuit losses as it dramatically underestimated the total experimental voltage (Fig. 3). Specifically, the difference of 92V between the calculated plasma voltage and the experimental total voltage suggests that such losses are of the order of 0.92MW, in other words almost half the available power is not deposited into the plasma and thus has no opportunity to be converted to useful thrust power. On the other hand, inclusion of such physics substantially elevated the plasma voltage (and thus plasma power deposition) implying that the

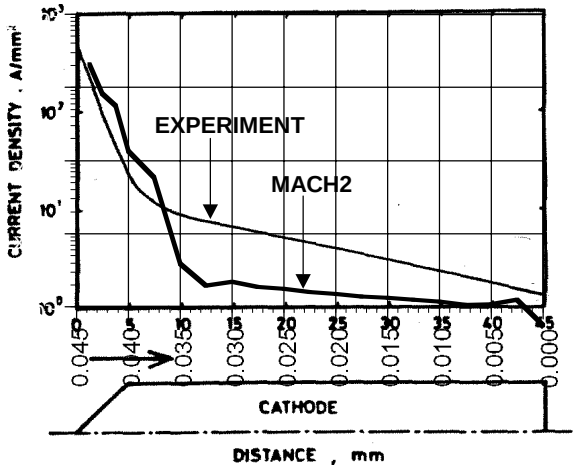

Figure 4. Current Density distribution over the cathode surface. (J=10kA)

predominant inefficiencies are due to frozen-flow losses. Furthermore, this is accurately illustrated by a power budget accounting for individual energy deposition to different modes and external losses. This is given below with the value in parenthesis corresponding to calculated values under classical transport:

Axial Thrust Power	= 0.5 MW	(0.377 MW)
Radial Thrust Power	= 0.123 MW	(0.08 MW)
Ionization Power	= 0.608 MW	(0.352 MW)
Thermal Power	= 0.445 MW	(0.251 MW)
Electrode Conduction	= 0.154 MW	(0.027 MW)
Fall Voltage Power	= 0.17MW	(0.92 MW)

The comparisons of the two-dimensional current distribution to experiment shown in Fig. 3 leave no doubt as to the validity of the formulation. Additional comparisons of the current distribution over the cathode, see Fig. 4, elaborates on the accuracy of the modeling and suggests the diminished contribution to energy losses through fall voltage. Due to fact that the current conduction zone is substantially downstream of the backplate

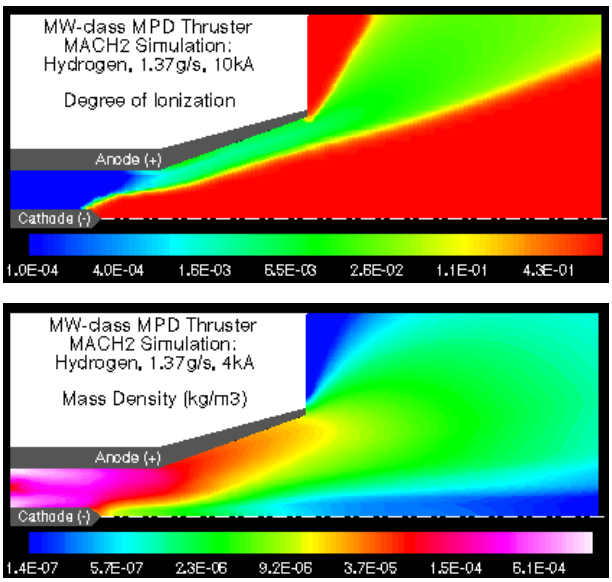

Figure 5. MACH2 two-dimensional distributions for the 10kA case. Top: Average degree of ionization. Bottom: Mass Density.

restricts power deposition via sheath falls to a smaller area - mainly the cathode-tip area - as opposed to the total electrode area. It should be noted that the logarithmic scale is responsible for an apparent discrepancy in the experimental and theoretical comparisons as we proceed toward the backplate. Even though, graphically the discrepancy appears substantial it does not exceed 1% of the maximum value. It is noteworthy that comparisons of the total thrust alone could not have offered such understanding or suggested inclusion of the improved model for the electrical diffusivity as both calculated thrust values can not be distinguished within experimental error.

Further support is provided by interrogation of the MACH2 calculated average degree of ionization which shows that ionization was less than 10^{-3} in the straight section of the discharge chamber proposing that electron-ion collisions do not dominate. The two-dimensional distribution shown in Fig. 5-top indicates that the propellant is significantly ionized far downstream of the backplate - which alleviates any concerns of the capability to numerically capture the short characteristic ionization scale-size evident in higher J^2/m thrusters - and only in the vicinity of the cathode tip and the lower-density zone extending downstream of the tip. This is also evident from examination of the mass density distribution, Fig. 5-bottom that displays most of the mass expanding through a region in the vicinity of the anode which should also be expected to be the main contributor to the total thrust. This in turn implies that a strong electrothermal component should be expected even at the higher power-level of 2 MW. (I.e. 10 kA case.)

Thrust and Voltage Comparisons

The overall trends of the performance of this version of the MY-II thruster and further understanding of the acceleration and power-loss mechanisms can be deduced from comparisons of the calculated and experimental thrust and voltage data for a range of discharge currents. The steady-state calculated thrust values are compared to the experimental ones in Fig. 6. They are very encouraging in both trends and magnitudes especially at the higher current levels. Some discrepancy is evident as power is decreased which is partly due to the possibility that even dissociation is incomplete at the exhaust region. This implies that the electrothermal component of the thrust would be reduced by the square root of the molecular weight and specific heat ratio, γ/γ-1 for molecular vs atomic hydrogen, i.e. a reduction of approximately 0.83.

The more revealing comparisons are those of experimental total voltage and MACH2-calculated plasma voltage, they are displayed in Fig. 7. The varying discrepancy with discharge current implies the relative losses due to fall voltage and frozen-flow. Specifically, at lower current levels the difference between plasma and total voltage is minimal suggesting that the main losses are due to energy deposition to the internal modes as opposed to sheath losses. As the power level is increased the discrepancy increases implying an increasing power deposition to the electrodes and a diminishing percentage to the internal energy modes; thermal, dissociation and ionization. This in turn can be related to the relative dominant thrust component as thruster operation transitions from mainly electrothermal to an electromagnetic accelerator. The argument can be further clarified by examining the ratio of electromagnetic thrust power to total thrust power, see Fig. 7, in relation to the voltage comparisons. The electromagnetic thrust power can be approximated by the Maecker formula which has

traditionally been used to estimate thrust:

$$P_{EM} = \frac{T^2}{2\dot{m}} \approx \left[\frac{\mu_o J^2}{4\pi} \left(\ln \frac{r_a}{r_c} + \frac{3}{4} \right) \right]^2 / 2\dot{m} \qquad (7)$$

It is noted that as P_{EM} / P_{THRUST} increases toward unity fall voltage losses become more significant (Total Voltage - Plasma Voltage) while for the same ratio being close to zero such losses are minimal if not non-existent. The latter can certainly occur if the plasma potential is equal to the electrode potential which in turn suggests avenues that can minimize sheath losses.

We can further examine the argument by comparing relative energy depositions for the extreme discharge current cases and the 10 kA case as follows:

Current (kA)	4	10	18
$(P_{INZ}+P_{THE}+P_{TBC})/P_{TOTAL}$	0.78	0.59	0.395
P_{FALL} /P_{TOTAL}	~0.0	0.083	0.18
P_{EM} /P_z	0.042	0.424	1.075

The ratio of power deposited to the internal energy modes and lost through electrode thermal conduction decreases with increasing current and power level while the projected fall voltage losses increase. This occurs as the thruster transitions from mainly electrothermal at 4 kA (P_{EM} /P_z=0.042) to approximately equally electrothermal and electromagnetic at 10 kA and mainly electromagnetic at 18 kA. (P_{EM} / P_z = 1.075. This is greater than one simply because the Maecker formula is an approximation with almost arbitrary choice of the additive term taken in eq. 7 as 3/4.) Thus, these comparisons suggest that the main losses during electrothermal operation are mainly frozen-flow losses which principally can be reduced by proper expansion of the flow, as in a converging-diverging nozzle. On the other hand, fall voltage losses increase with power level, however, for this thruster's operation regime and geometry they are not detrimental and any frozen-flow recoveries from proper nozzle design will benefit its performance. This is of course due to the fact that the thruster operates in a regime that plasma resistivity is dominated by an additive term due to atom-electron collisions which in turn elevates the power deposited to the plasma and minimizes sheath losses. In turn, it provides the opportunity to recover some of the energy to useful thrust as opposed to alternate operations during which the major percentage of the available power can not deposited to the plasma, but rather it is expended to the electrodes via fall voltage losses.

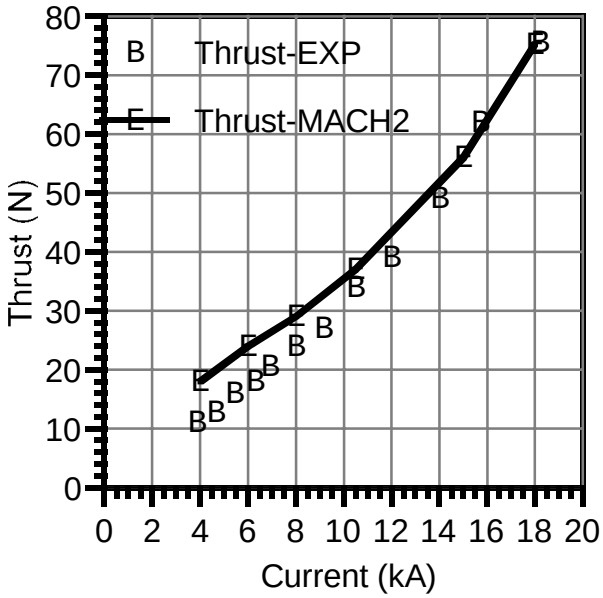

Figure 6. Comparisons of the MACH2- calculated thrust with experimental data for a range of discharge currents.

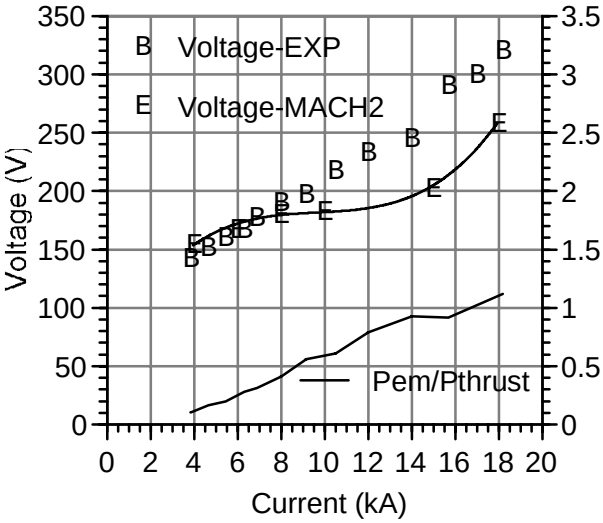

Figure 7. Comparisons of calculated plasma voltage to experimental total voltage. The ratio of electromagnetic thrust power to total thrust is also depicted.

Conclusions

Numerical simulations of a MW-class, self-field MPD thruster were performed with the MACH2 code in order to validate the model and provide useful insights toward improving performance. Experimental data for thrust, voltage and current distribution were available for the necessary comparisons which were very convincing regarding the validity of the physical model. Two-dimensional current distribution comparisons determined that modeling with classical transport is inadequate, rather atom-electron collisions dominate in such a manner so as to substantially increase the plasma resistivity. This in turn predicted elevated plasma power deposition and minimal electrode losses due to fall voltage. The dominant energy deposition was calculated to be frozen-flow even though it decreased with increasing discharge current. It is thus deduced that significant performance improvements can be achieved by expanding the flow through an appropriately designed converging-diverging nozzle.

References

1. Sovey, J.S. and Mantenieks, M.A. "Performance and Lifetime Assessment of MPD Arc Thruster Technology," NASA Technical Memorandum 101293, AIAA-88-3211, 24th Joint Propulsion Conference, Boston, MA, 1988.

2. Myers, R.M., Mantenieks, M.A. and LaPointe, M.R., "MPD Thruster Technology," NASA Technical Memorandum 105242, AIAA-91-3568, Conference on Advanced Space Exploration Initiative Technologies, 1991.

3. Uematsu, K.J., Mori, K., Kunikaka, H., and Kuriki, K., "Effects of Electrode Configuration on MPD Arcjet Performance," 17th International Electric Propulsion Conference, Japan Society for Aeronautical and Space Sciences, Tokyo, 1984, pp. 79-86.

4. Burton, R.L., Clark, K.E., and Jahn, R.G. "Measured Performance of a Multimegawatt MPD Thruster," *Journal of Spacecraft and Rockets*, Vol. 20, No. 3, pp. 299-304, May-June 1983.

5. Peterkin, R.E. and Frese, M.H., MACH: A Reference Manual – First Edition, Air Force Research Laboratory, Kirtland AFB, New Mexico, September 14, 1998.

6. Frese, M.H., "MACH2: A Two-Dimensional Magnetohydrodynamics Simulation Code for Complex Experimental Configurations," AMRC-R-874, September 1986.

7. Peterkin, R.E., Jr., and Frese, M.H., "A Material Strength Capability for MACH2," MRC/ABQ-R-1191, October 1989.

8. Mikellides, P.G., "A Theoretical Investigation of Magnetoplasmadynamic Thrusters," Ph.D. Dissertation, Department of Aeronautical and Astronautical Engineering, The Ohio State University, 1994.

9. Turchi, P.J. Mikellides, I.G. Mikellides, P.G. and H. Kamhawi, "Pulsed Plasma Thrusters for Microsatellite Propulsion: Techniques for Optimization," Micro-Propulsion for Small Spacecraft, *Progress in Astronautics and Aeronautics*, Hardcover ISBN: 1-56347-448-4 , Copyright 2000.

10. Braginskii, S.I., "Transport Processes in a Plasma," in *Review of Plasma Physics*, M.A. Leontovich, ed. Consultants Bureau, New York, 1965.

11. Douglas, M.R., "Radiation Production from Stagnating Compact Toroids Employing a Nonequilibrium Radiation Diffusion Model," Ph.D. Dissertation, U. of New Mexico, 1994.

12. Holian, K.S., ed, "T-4 Handbook of Material Properties Data Base.. Vol Ic: EOS," LA-1160-MS, Los Alamos National Laboratory, Los Alamos, NM, November, 1984.

13. Buff, J. et. al., "Enhancement of the Radiation Yield in Plasma Flow Switch Experiments," MRC/ABQ-R-1171, Mission Research Corporation, Albuquerque, NM, 1988. Also see: *IEEE Transactions on Plasma Science*, 15, 6, pp. 766-771, 1987.

14. Peterkin, R.E., Jr., et. al., “Simulations of Staged Solid Shell Implosions to Produce Fusion,” AIAA Pre-print 95-2899, 31st AIAA Joint Propulsion Conference and Exhibit, San Diego, CA, 1995.

15. Degnan, J.H., Peterkin, R.E., Jr. et. al., “Compact Toroid Formation, Compression, and Acceleration,” *Physics of Fluids*, B5 (8), 2938, 1993.

16. Degnan, J.H., et. al., “Electromagnetic Implosion of Spherical Liner,” *Phys. Rev. Lett.*, 74 (1), 98, 1995.

17. Stamper, J.A., et. al., “Aneurysms in laser-driven last waves,” *Physics of Fluids*, 31 (11), 3353, 1988.

18. Mikellides, P.G., Turchi, P.J., and Mikellides, I.G., "Design of a Fusion Propulsion System, Part 1: Gigawatt-Level Magnetoplasmadynamic Source,” *Journal of Propulsion and Power*, submitted Sept. 2000. Log No. B4106. IEPC Preprint 99-013.

19. Mikellides, I.G., Mikellides, P.G., Turchi, P.J. and York, T.M."Design of a Fusion Propulsion System, Part 2: Numerical Simulation of Magnetic-Nozzle Flows," *Journal of Propulsion and Power*, submitted Sept. 2000. Log No. B4107. AIAA Preprint 00-3367.

20. Tahara, H., Kagaya, Y. and T. Yoshikawa, “Quasi-Steady MPD Arcjets with Applied Magnetic Fields,” AIAA-85-2001, 18th International Electric Propulsion Conference, Alexandria, VA, 1985.

21. Tahara, H., Kagaya, Y. and Yoshikawa, T. “Quasi-Steady Magnetoplasmadynamic Thrusters with Applied Magnetic Fields for Near-Earth Missions,” *Journal of Propulsion*, 5 (6), 713, Nov.-Dec. 1989.

22. Brode, R.B., Energy Dependence of electron-atom elastic cross sections, *Review in Modern Physics*, 5 p. 257, 1933.